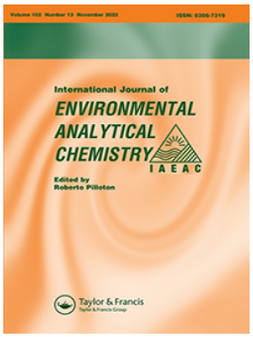

International Journal of Environmental Analytical Chemistry

ISSN: (Print) (Online) Journal homepage: https://www.tandfonline.com/loi/geac20

Cobalt aluminate/carbon nanocomposite via an auto-combustion method: an efficient photocatalyst for photocatalytic degradation of organic dyes from aqueous media

Meshari M. Aljohani, Emad M. Masoud, Naglaa M. Mohamed & Mostafa Y. Nassar

To cite this article: Meshari M. Aljohani, Emad M. Masoud, Naglaa M. Mohamed & Mostafa Y. Nassar (2021): Cobalt aluminate/carbon nanocomposite via an auto-combustion method: an efficient photocatalyst for photocatalytic degradation of organic dyes from aqueous media, International Journal of Environmental Analytical Chemistry, DOI: 10.1080/03067319.2021.1979533

To link to this article: https://doi.org/10.1080/03067319.2021.1979533

Published online: 20 Sep 2021.

INTERNATIONAL JOURNAL OF ENVIRONMENTAL ANALYTICAL CHEMISTRY
https://doi.org/10.1080/03067319.2021.1979533

Taylor & Francis
Taylor & Francis Group

Cobalt aluminate/carbon nanocomposite via an auto-combustion method: an efficient photocatalyst for photocatalytic degradation of organic dyes from aqueous media

Meshari M. Aljohani[a], Emad M. Masoud[b,c], Naglaa M. Mohamed[b] and Mostafa Y. Nassar[b]

[a]Chemistry Department, Faculty of Science, University of Tabuk, Tabuk, Saudi Arabia; [b]Chemistry Department, Faculty of Science, Benha University, Benha, Egypt; [c]Chemistry Department, Faculty of Science, Islamic University of Madinah, Madinah, Kingdom Saudi Arabia

ABSTRACT

Cobalt aluminate/carbon composite nanoparticles have been synthesised by utilising an auto-combustion method using glycine as an inexpensive fuel. The products were analysed by various techniques such as powder X-ray diffraction (XRD), Fourier transform infrared (FT-IR), thermal analysis (TG), field emission scanning electron microscopy (FE-SEM), transmission electron microscopy (TEM), and X-ray photoelectron spectroscopy (XPS), UV-Vis diffuse reflectance spectrum (DRS), energy-dispersive X-ray spectroscopy (EDS). The results exhibited that the average crystallite size of the as-prepared $CoAl_2O_4$/C nanocomposite was ca. 26 nm. The photocatalytic activity of the as-prepared catalyst was evaluated through the degradation of methylene blue (MB) dye under different conditions, and the photocatalytic degradation mechanism was proposed. The results indicated that $CoAl_2O_4$/C nanocomposite has a high catalytic performance for the photocatalytic degradation of MB dye under UV illumination in the presence of H_2O_2. The degradation efficiency reached 98.5% in 90 min with a degradation rate constant of 0.046 min^{-1}.

ARTICLE HISTORY
Received 16 March 2021
Accepted 1 September 2021

KEYWORDS
Cobalt aluminate/carbon nanocomposite; photocatalysis; hydrogen peroxide; methylene blue dye

1. Introduction

Dyeing processing in various industries such as paper, plastic, textile, rubber, etc. is still one of the great major resources for water pollution because most factories discharge their waste including dyes into the environment without treatment [1,2]. Most of those dyes are harmful to the environment due to their toxicity and carcinogenicity [3]. For instance, methylene blue dye (MB) is extensively used in the silk, wool, and cotton industry, and this dye results in serious human health issues such as nausea, vomiting, difficulty in breathing, methemoglobinemia, mental confusion as well as various aquatic ecosystem problems [4–6]. Hence, exploring a method to eliminate these pollutants is an indispensable task for researchers [7–10]. In this regard, several physical, biological, and chemical methods have been suggested

CONTACT Mostafa Y. Nassar m_y_nassar@fsc.bu.edu.eg; Emad M. Masoud emad_masoud1981@yahoo.com

for removing pollutants from wastewater such as biological treatment, electrochemical and ultrasonic technique, precipitation, adsorption, filtration, chemical oxidation, solvent extraction, coagulation, reverse osmosis, and membrane process [1,11–14]. However, these methods are expensive, and they usually displayed ineffectiveness at low concentrations [15]. Lately, photocatalytic degradation using semiconductors continues to draw considerable consideration due to its high ability to degrade numerous resistant and hazardous organic contaminants such as dyes [16–19]. Meanwhile, the synthesis of several semiconductor nanomaterials of diverse size, composition, structure, and morphology has been developed as photocatalysts for the removal of organic pollutants attributing to their facile synthetic methods and interesting optical properties [20–24]. Moreover, advanced oxidation processes (AOPs) have been substantiated to be one of the most effective routes for removing organic contaminants from wastewater; where, the highly reactive hydroxyl radicals ($^{\bullet}OH$) are generated and bring about the oxidative degradation of organics [25,26]. Degradation of pollutants by nanocatalyst/H_2O_2 process has recently received significant attention attributing to its low cost and high efficiency [27,28]. In this respect, several catalysts such as H_2O_2/UV [29], Fenton and Fenton-like reactions: (Fe^{2+}/H_2O_2) [30], H_2O_2/O_3 [31], Fe_3O_4/H_2O_2 [32,33] and CuO/H_2O_2 [34], were applied in the presence of hydrogen peroxide to enhance the degradation efficiency of the pollutants. Furthermore, spinel structured oxide materials have gained considerable attention because of their interesting catalytic properties [35–37]. Among nanostructured spinel oxides, cobalt aluminate has received a research focus due to its thermal and chemical stability as well as its desirable catalytic and optical characteristics [38,39]. As such, various routes have been adopted for the synthesis of cobalt aluminate such as microwave [40], co-precipitation [41–43], hydrothermal [44], sol-gel [38,45,46], and combustion technique [47,48]. However, the combustion approach has attracted the keen interest of several research groups, owing to its low cost, feasibility, and scalability [16]. In addition, reports on the synthesis of cobalt aluminate through a combustion method are limited [49]. Besides, it was reported that $CoAl_2O_4$ was used as a catalyst with hydrogen peroxide for the highly selective oxidation of benzyl alcohol to benzaldehyde with high efficiency [40]. Moreover, previous research demonstrated that $ZnO/Zn_2TiO_4/C$ and $TiO_2/Zn_2TiO_4/ZnO/C$ composites are efficient photocatalysts under solar and/or UV irradiation [16,50]. This background stimulated us to fabricate $CoAl_2O_4/C$ nanocomposite at a relatively low temperature via an auto-combustion synthetic method and explore its efficiency as a photocatalyst with the help of H_2O_2 existence. Therefore, we herein have developed an auto-combustion method for the synthesis of $CoAl_2O_4/C$ nanocomposite using glycine as an inexpensive fuel. The efficiency of the as-prepared $CoAl_2O_4/C$ as a photocatalyst for the removal of methylene blue (MB), as a pollutant model, under UV irradiation in the presence of H_2O_2 was extensively explored. The chemical kinetics of the photocatalysis process of MB dye was also investigated.

2. Experimental

2.1. Materials and reagents

Cobalt nitrate ($Co(NO_3)_2 \cdot 6H_2O$), aluminium nitrate ($Al(NO_3)_3 \cdot 9H_2O$), glycine (NH_2CH_2COOH), and methylene blue (MB) dye ($C_{16}H_{18}ClN_3S$) were purchased from Sigma-Aldrich Company (USA) and used without further purification.

2.2. Synthesis of cobalt aluminate/carbon nanocomposite

Cobalt aluminate/carbon nanocomposite was prepared via an auto-combustion method using glycine as a fuel. In this procedure, the applied quantities of the reactants were based on the basis that the equivalence ratio, Φ_c, should equal unity (i.e. $\Phi_c = (F/O) = 1$) to maximise the released energy from the combustion process for the reaction. Where (F) is the total fuel reducing valence and (O) is the total oxidant oxidising valence (i.e. cobalt nitrate + aluminium nitrate) [51]. In a typical preparation: at room temperature, a glycine aqueous solution (2.00 g, 26.6 mmol, 30 mL) was added to a stirring aqueous solution (40 mL) of a mixture of cobalt nitrate ($Co(NO_3)_2.6H_2O$; 1.75 g, 6.00 mmol) and aluminium nitrate ($Al(NO_3)_3 \cdot 9H_2O$; 4.50 g, 12.0 mmol). The used molar ratio of Co^{2+}: Al^{3+} was 1:2. The reaction mixture was allowed to stir at room temperature for 10 min to obtain a homogenous solution. The reaction blend was then stirred at 100°C until a viscous liquid was produced. Thereafter, the temperature was increased to ca. 300°C, during which the entire combustion was taken place in ca. 5 min. The ignited precursor was ground and calcined at 600°C for 2 h to give cobalt aluminate/carbon nanocomposite product.

2.3. Photocatalytic activity investigation

The photocatalytic activity of the as-prepared cobalt aluminate/C nanocomposite towards the degradation of methylene blue (MB) dye was performed in a Pyrex beaker under UV illumination using a 250 W xenon arc lamp (Toshiba, SHLS-002) (λ = 365 nm) at room temperature (25°C) and neutral pH. The photocatalytic degradation of MB dye on cobalt aluminate/C photocatalyst was carried out as follows: In brief, 0.03 g of the as-synthesised nanocomposite photocatalyst was added to 50 mL of MB aqueous solution (20 mgL^{-1}) under continuous stirring. Prior to UV illumination and under dark conditions, the suspension was continuously stirred for about 30 min to reach an adsorption-desorption equilibrium between MB dye and the photocatalyst. Afterwards, 0.4 mL H_2O_2 (30 wt.%, Adwic company, Egypt) was added and the aqueous dye solution was then irradiated with UV light illumination under continuous stirring. At given time intervals, the decomposed dye sample was periodically taken out and centrifuged to separate out the nanocomposite. The concentrations of the remaining dye after degradation were analysed by measuring the absorbance of the MB dye at λ = 663 nm using a UV–Vis spectrophotometer (JASCO V-670, Japan). The percentage of degradation can be calculated using the following equation, with the help of a pre-constructed calibration curve for MB dye of different concentrations:

$$\%\text{degradation} = [(C_o - C)/C_o] \times 100$$

Where C_o is the initial concentration at 0 min, and C is the concentration at time t. To investigate the effect of H_2O_2 on the catalytic performance of the nanocomposite, similar experiments were also carried out for the degradation process of the MB dye using the following: a) $CoAl_2O_4$/C catalyst + dark; b) $CoAl_2O_4$/C catalyst + UV; c) UV only; d) H_2O_2+ dark; e) $CoAl_2O_4$/C catalyst + H_2O_2 + dark; f) H_2O_2 + UV; and g) $CoAl_2O_4$/C catalyst + H_2O_2 + UV.

Moreover, the kinetics of the photocatalytic degradation of MB dye was examined using the pseudo-first-order model, and the apparent rate constant, k, was determined using the following relation:

$$\ln(C_o/C) = kt$$

The k constant value was obtained from the plot of $\ln(C_o/C)$ against time intervals; where C_o and C have the aforementioned meaning.

2.4. Physico-chemical measurements

The powder X-ray diffraction analysis of the as-fabricated product was carried out on a Diano (made by Diano Corporation, USA). The diffractometer was equipped with Cu-filtered CuKα radiation (λ = 1.5418 Å) energised at 45 kV, and 10 mA. The sample was measured, at room temperature, in the range 2θ = 10 to 80°. The sample infrared spectrum was measured in the range of 400–4000 cm^{-1} utilising an FT-IR spectrometer (Thermo Scientific, model Nicolet iS10). Thermal stability of the as-prepared $CoAl_2O_4$/C nanocomposite was performed using a thermal analyser instrument (Shimadzu; model TA-60WS) under nitrogen gas atmosphere at 15 °C/min heating rate in a temperature range of 25–1000°C. X-ray photoelectron spectroscopy (XPS) was measured using an ESCALAB 250 spectrometer with monochromatized Al Kα X-ray radiation in ultra-high vacuum (<10 − 7 Pa). The morphology of the as-prepared nanocomposite was examined using a field emission scanning electron microscope (FE-SEM; JEOL, model JSM-6390), and a high-resolution transmission electron microscope (HR-TEM; model JEM-2100) equipped with an accelerating voltage of 200 kV equipped with energy-dispersive X-ray spectrometer (EDS spectrometer). The $CoAl_2O_4$/C nanocomposite UV-Vis diffuse reflectance spectrum was recorded using UV-visible spectrophotometer (Jasco, model v670) equipped with an integral sphere (Jasco, model ISN-723). The concentration of the methylene blue dye was determined using a UV-visible spectrophotometer (Jasco, model v670).

3. Results and discussion

3.1. Synthesis and characterisation of $CoAl_2O_4$/C nanocomposite

$CoAl_2O_4$/C nanocomposite was synthesised via an auto-combustion method utilising a mixture of cobalt nitrate and aluminium nitrate as an oxidant and a glycine fuel as a reductant. The applied fuel-to-oxidant relative ratio was 4.44 to get the maximum released energy from the current combustion reaction. Scheme 1 exhibited the proposed combustion reaction of the used metal nitrates and the glycine fuel. The ignited and calcined composites were identified employing various techniques including XRD, FT-IR, thermogravimetric analysis, SEM, EDS, TEM, and diffuse reflectance spectroscopy, as shortly will be explained.

3.1.1. XRD investigation

XRD analysis was performed to investigate the crystal phase of the as-prepared product calcined at 600°C, as shown in Figure 1. The observed diffraction peaks at 2θ = 31.32°, 36.90°, 44.88°, 55.65°, 59.45°, and 65.25° can be assigned to cubic spinel $CoAl_2O_4$ product with (220), (311), (400), (422), (511), and (440) crystallographic planes, respectively, (JCPDS

$$9Co(NO_3)_2.6H_2O(aq) + 18Al(NO_3)_3.9H_2O(aq) + 40\ C_2H_5NO_2(aq) \longrightarrow 9CoAl_2O_4(s) + 56N_2(g) + 80CO_2(g) + 316H_2O(g)$$

Scheme 1. Proposed combustion reaction of cobalt nitrate and aluminium nitrate with glycine fuel.

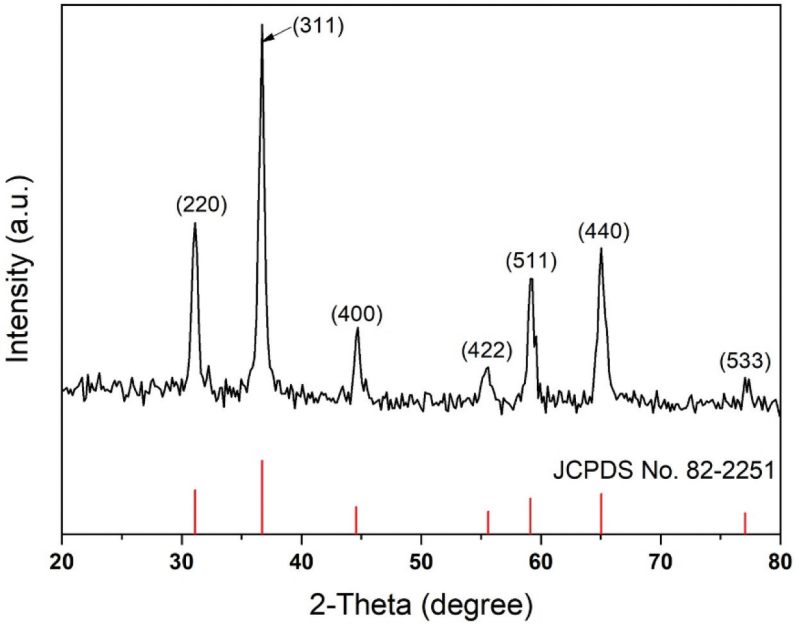

Figure 1. X-ray diffraction pattern of the as-prepared $CoAl_2O_4$ nanoparticles.

File No. 82–2251), indicating the successful synthesis of $CoAl_2O_4$ product via the combustion method. No other crystalline phases are detected in the XRD pattern, supporting the purity of the prepared sample. The average crystallite size of the obtained $CoAl_2O_4$ product was estimated to be ca. 26 nm, using the following Debye-Scherrer equation [23,52]:

$D = 0.9\lambda/\ \beta\ \cos\theta_B$

where, θ_B is the Bragg diffraction angle, λ (nm) is the wavelength of the used X-ray radiation, and β is the diffraction peak full width at half maximum (FWHM).

3.1.2. FT-IR investigation

The bonding and chemical composition of the as-prepared $CoAl_2O_4$/C product were studied using FT-IR spectroscopy, as displayed in Figure 2. The bands appeared at ca. 3471.5 and 1650 cm^{-1} are probably attributed to the stretching and bending vibrations of the hydrogen-bonded OH groups and/or surface adsorbed water molecules [15,53]. The absorption bands at 2910.2, 1556.9, 1441.9, and 1104.7 cm^{-1} can be assigned to various carbon residue stretching vibrations including C-H, C = C, O-C-O, and C-O-C and others [54]. It is worth mentioning that these vibration bands present in the product even after

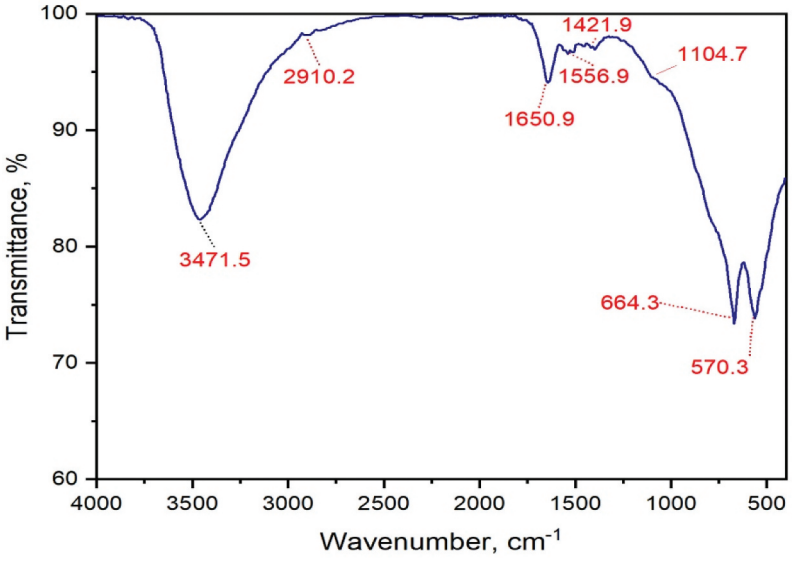

Figure 2. FT-IR spectrum of the as-prepared $CoAl_2O_4$/C nanocomposite.

calcination at 600°C, and this is consistent with published data [55]. The bands over the range of 1000–400 cm^{-1} (664.3 and 570.3 cm^{-1}) correspond to stretching vibration of the metal-oxygen bonds (i.e. Co-O and Al-O) of the spinel $CoAl_2O_4$ structure of the as-prepared product that is already confirmed by XRD data [40,49]. Therefore, the FT-IR results substantiate the formation of $CoAl_2O_4$/carbon residue nanocomposite [16].

3.1.3. Thermal analysis

The thermal behaviour of $CoAl_2O_4$/C nanocomposite was investigated by TG technique and presented in Figure 3. The TG curve exhibited mass loss steps at ca. 92, 263, and 700°C with an overall mass loss of 9.7%. The first weight loss step (2.83%), in the region 25–137°C, can be ascribed to the volatilisation of free and adsorbed water molecules existing in the sample. The second weight loss (4.24%), in the temperature region 137–455°C, is a complex step and it is composed of at least two overlapped steps. This step is probably due to the loss of interlayer water molecules and the oxidative thermal decomposition of some cobalt and aluminium nitrates and the glycine fuel [56]. The third weight loss (2.63%), in the temperature region 455–800°C, is also a complex step, and it is probably attributed to the decomposition of the remaining metal nitrates residue and organic matter, leaving pure $CoAl_2O_4$ nanoparticles with some carbon residue. It should be noted that the sample at even higher temperatures (800°C) did not reach a constant weight, supporting the existence of the carbon residue in the $CoAl_2O_4$ product. These results are compatible with the FT-IR data.

3.1.4. Morphology investigation

The morphology of the as-prepared $CoAl_2O_4$/C nanocomposite was investigated using field FE-SEM, EDS, and TEM techniques as presented in Figure 4. The FE-SEM micrograph (Figure 4(a)) of the $CoAl_2O_4$/C nanocomposite exhibited that the product consisted of

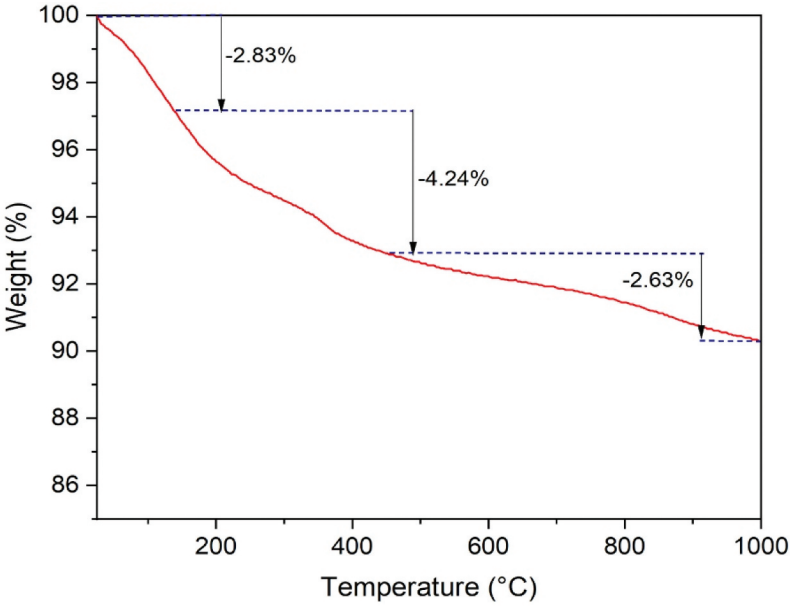

Figure 3. Thermogravimetric analysis (TG) of the as-prepared $CoAl_2O_4$/C nanocomposite.

spherical and irregular particles. There are some dark spots, which may be due to the presence of some carbon residue in the product. The EDS spectrum (Figure 4(b)) of the product assured that the product is composed solely of cobalt, aluminium, and oxygen elements. Besides, the spectrum showed also the presence of the carbon element in the $CoAl_2O_4$ sample, which is consistent with our previous results. The TEM image of the as-prepared nanocomposite revealed that $CoAl_2O_4$/C nanocomposite is composed of spherical, hexagonal, and irregular particles of $CoAl_2O_4$, as well as some of those particles are covered with a thin layer of carbon residue, deduced from the dark colour surrounded some particles. The TEM image also revealed that the average particle is ca. 27 nm, which is consistent with the XRD results.

3.1.5. XPS investigation

The XPS analysis is widely utilised to identify the surface, oxidation states, and chemical states of the elements of the as-prepared cobalt aluminate nanostructures. The XPS spectra of the as-prepared $CoAl_2O_4$/C nanocomposite are presented in Figure 5. The XPS spectrum (Figure 5 (a)) revealed the elemental peaks for Co 2p, Al 2p, and O 1s, confirming the formation of $CoAl_2O_4$ nanostructure. Besides, Figure 5 (b) showed doublet peaks of Co $2p_{1/2}$ and Co $2p_{3/2}$, attributing the binding energies 794.51 eV and 778.83 eV respectively. This supports the presence of Co^{2+} ions in the tetrahedral sites of the spinel $CoAl_2O_4$. While the octahedral sites of the spinel $CoAl_2O_4$ occupied by Al^{3+} ions appeared at 73.26 eV as assured by Al 2p spectrum (Figure 5(c)) [57,58]. Figure 5(d) revealed a peak at a binding energy of 529.32 eV, which may correspond to O atoms of the spinel $CoAl_2O_4$ product and the physically adsorbed water molecules on the product [58]. Furthermore, Figure 5(e) exhibited the presence of C 1s peak which is overlapped with another small peak that

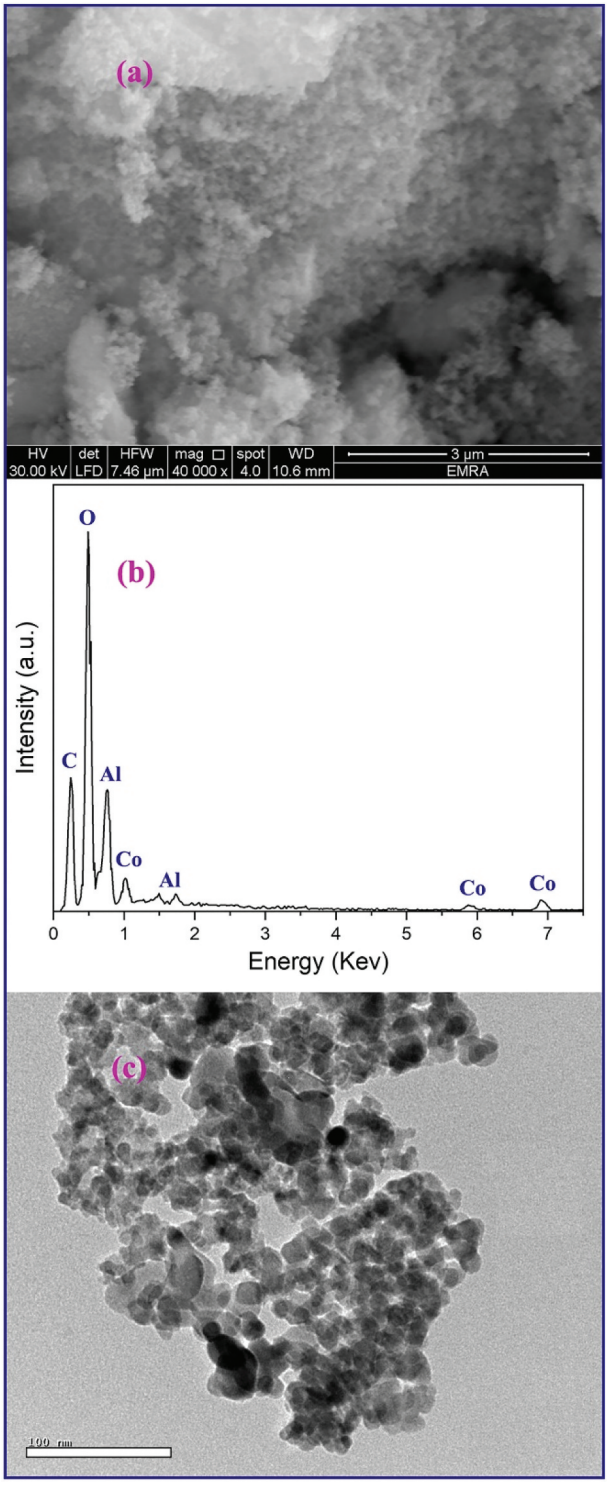

Figure 4. FE-SEM image (a), EDS spectrum (b), and TEM image (c) of the as-prepared $CoAl_2O_4$/C nanocomposite.

appeared as a shoulder at a binding energy of 283.28 eV and 288.1 eV, which may correspond to the presence of a small amount of carbon residue (C-C and C-OH/C = O, respectively) as a kind of contamination in the $CoAl_2O_4$ product [17]. This indicates that some of $CoAl_2O_4$ nanoparticles are covered by a thin layer of carbon residue, and this is in a good agreement with the published data [50]. Moreover, the results are in consistent with those obtained from FT-IR and thermal analysis, which all confirm the formation of $CoAl_2O_4$/C nanocomposite.

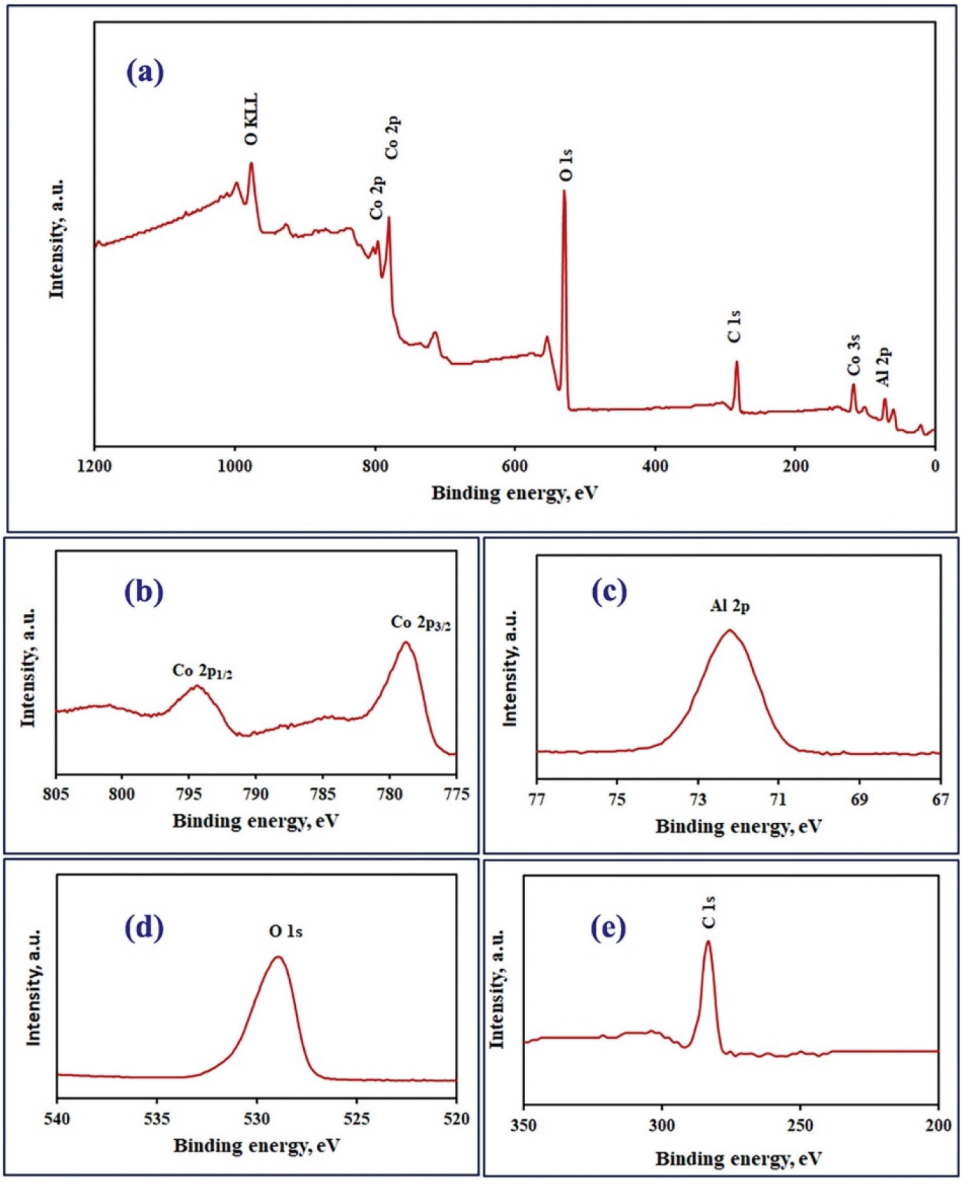

Figure 5. XPS survey spectra (a) and high resolution XPS spectra of Co 2p (b), Al 2p (c), O 1s (d), and C 1s (e) of the as-prepared $CoAl_2O_4$/C nanocomposite nanoparticles.

3.1.6. Optical properties

The optical properties of the nanocrystalline $CoAl_2O_4$ spinel have been investigated by measuring its UV-Vis diffuse reflective spectrum (DRS) (Figure 6). The measured DRS spectrum (Figure 6(a)) was utilised to determine the optical energy band gap value from the Tauc relationship [59]. In this regard, Kubelka–Munk function F(R) was applied to convert the diffused reflectance (R) into the absorption coefficient (α), as represented in the following equation:

$$\alpha = F(R) = \frac{(1-R)^2}{2R}$$

Therefore, the Tauc equation can be written as follows: $[F(R)x\hbar\upsilon] = K(\hbar\upsilon - E_g)^n$

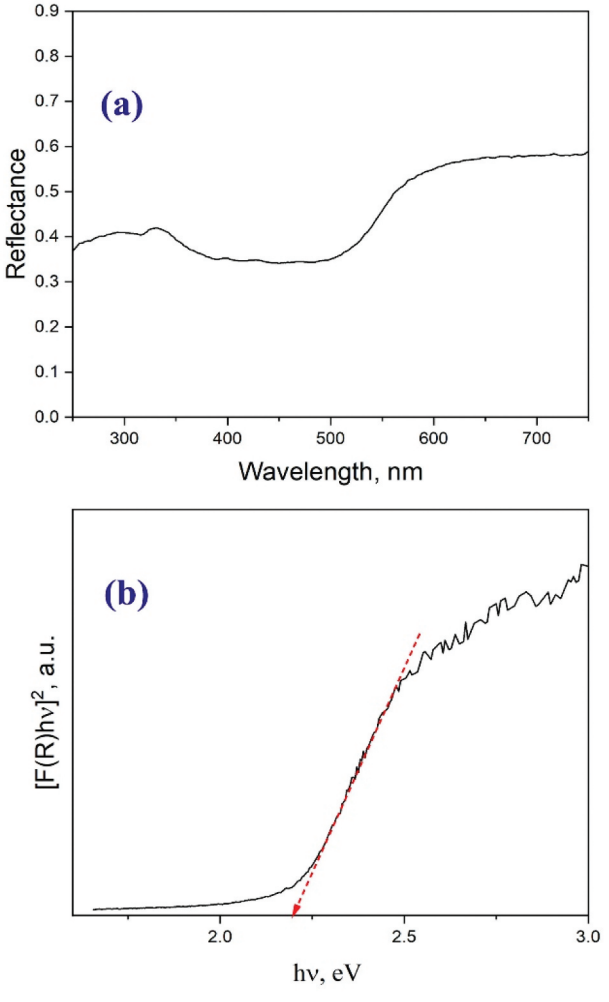

Figure 6. UV-Diffuse reflectance spectrum (a), and plot $[F(R)x\hbar\upsilon]^2$ against $\hbar\upsilon$ (b) of the as-prepared $CoAl_2O_4$/C nanocomposite.

Where K is constant, E_g is the optical band gap energy, and hυ is the energy of the incident photon in eV. Besides, n = 2 and 1/2 for the allowed direct and indirect transitions, generating direct and indirect band gaps, respectively. The direct band gap energy of the $CoAl_2O_4$ product is determined by plotting $[F(R)xh\upsilon]^2$ against hυ (Figure 6(b)). The band gap energy value (E_g) of the $CoAl_2O_4$ product can be calculated from the extrapolation of the linear section of the plot at $[F(R)xh\upsilon]^2 = 0$. The band gap energy value (E_g) was estimated to be 2.2 eV, which is compatible with the reported ones [60].

3.2. Photocatalytic activity of $CoAl_2O_4$/C nanocomposite

The MB dye degradation catalysed by the as-synthesised $CoAl_2O_4$/C nanocomposite was investigated under different conditions to explore the photocatalytic activity. The UV-Vis spectra of MB solution during this study were recorded in the wavelength range from 400 to 800 nm. Figure 7 shows the UV-Vis absorption spectra of MB solutions containing the as-prepared $CoAl_2O_4$/C nanocomposite and H_2O_2 with the variation of UV illumination time from 0 to 101 min, and they exhibit the maximum absorption at a wavelength of ca 663 nm. From Figure 7, it can be seen that the absorption intensities of MB dye continuously decrease with the increase of exposure time corresponding to the decrease in MB dye concentration.

It is worth mentioning that the MB dye degrades in this case by ~ 98.5% within a short exposure time of 90 min. Moreover, Figure 8 shows the relative concentration of MB (C/C_o) at different time intervals under different conditions. It is clearly seen from Figure 8 (a) that the dye removal percentage was about 5% in the dark and in the absence of H_2O_2, due to the adsorption of MB dye on $CoAl_2O_4$/C nanocomposite after the adsorption equilibrium was reached. Moreover, under UV irradiation only, the photocatalyst was ineffective and the dye removal percentage was about 6.1%, Figure 8 (b). Additionally, the relative concentration of MB (C/C_o) at different time

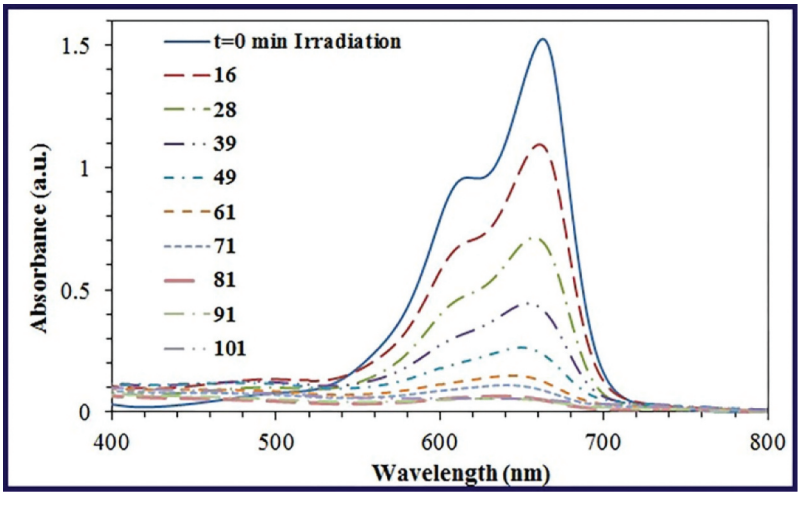

Figure 7. UV-Vis absorption spectra of MB solution containing $CoAl_2O_4$/C nanocomposite and H_2O_2 at different UV illumination time periods. Reaction conditions: MB = 20 mgL^{-1}, catalyst = 0.03 g, H_2O_2 (30%) = 0.4 mL, pH = neutral, and temperature = 25°C.

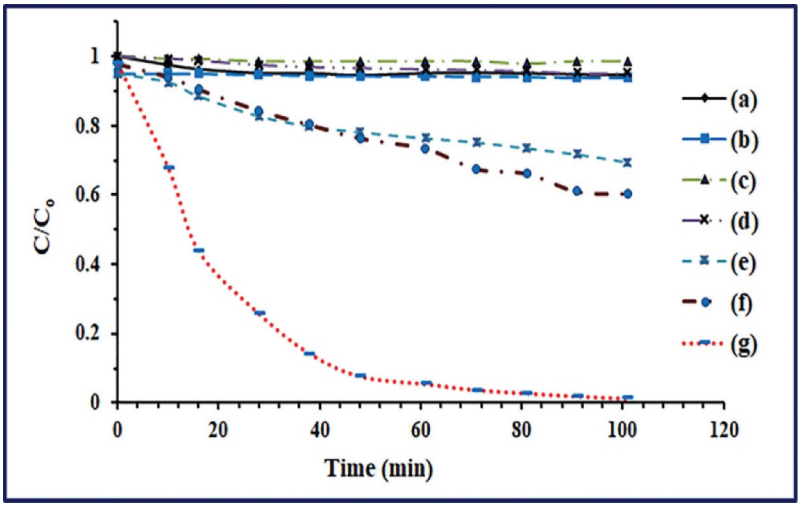

Figure 8. Relative concentration (C_0/C) of MB solution against time at the following different conditions: a) $CoAl_2O_4$/C catalyst + dark; b) $CoAl_2O_4$/C catalyst + UV; C) UV only; d) H_2O_2 + dark; e) $CoAl_2O_4$/C catalyst + H_2O_2 + dark; f) H_2O_2 + UV; and g) $CoAl_2O_4$/C catalyst + H_2O_2 + UV.

intervals in the dark remained nearly constant in the presence of H_2O_2 and absence of $CoAl_2O_4$/C nanocomposite, as displayed in Figure 8 (d), concluding that H_2O_2 alone can almost not degrade the MB dye under the used experimental conditions. Besides, Figure 8(c) exhibited that the MB degradation ratio was negligible (<1.5%) under the UV irradiation in the absence of the photocatalyst and H_2O_2.

In addition, the degradation efficiency of MB dye has been performed approximately 27% after 90 min in the presence of the catalyst, H_2O_2, and dark (heterogeneous Fenton-like reaction), as shown in Figure 8(e). This indicated that $CoAl_2O_4$ was not completely active towards the H_2O_2 reaction. However, the degradation efficiency of MB reached about 39% after 90 min UV irradiation in the presence of H_2O_2 only [Figure 7(f)]. This can be attributed to the photolysis of H_2O_2 into $^{\bullet}OH$ radicals, which in turn may oxidise MB dye molecules. On the other hand, photocatalysis of MB dye using the as-prepared catalyst in the presence of H_2O_2 and UV irradiation was the most effective in photodecomposition of MB which as previously mentioned reached about 98.5% in only 90 min of UV irradiation, Figure 8(g).

The kinetic behaviour of the noticeable photodegradation processes indicated from Figure 8 (e-g) was investigated. A plot of $\ln(C_o/C)$ versus t is linear, and the curves are presented in Figure 9(a-c), where t is the contact time [Figure 9 (c)] or the irradiation time [Figure 9(a,b)], respectively. Generally, good correlations were obtained, suggesting the degradation reaction kinetics follow a pseudo-first-order rate law. From the slope of the lines in Figure 9 (a-c), the rate constant of MB degradation for the catalyst + H_2O_2 + UV irradiation, (Figure 9b), was calculated to be 0.046 min^{-1}; and for H_2O_2 + UV irradiation only, (Figure 8a), was found to be 0.0046 min^{-1}; while that in the presence of the catalyst + H_2O_2 + dark, (Figure 9c), reached 0.0032 min^{-1}. The pseudo-first-rate constant (i.e. the degradation in the presence of catalyst + H_2O_2 + UV irradiation) was 10 times more than the second and ~ 14 times more than the last one.

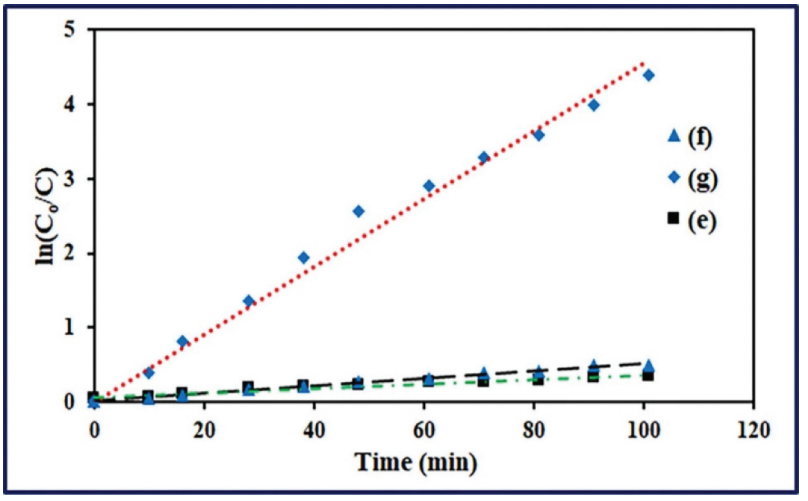

Figure 9. Relative concentration [$\ln(C_0/C)$] of MB solution against time at different conditions: a) H_2O_2 + UV; b) $CoAl_2O_4$/C catalyst + H_2O_2 + UV; and C) in dark and presence of H_2O_2 and catalyst.

3.3. Study of the reactive species and the proposed photodegradation mechanism

To explore the photodegradation mechanism of MB dye in the presence of $CoAl_2O_4$ /C catalyst + UV + H_2O_2, the reactive species (h^+, $O_2^{\bullet-}$, and $^{\bullet}OH$) were monitored by utilising three selective radical scavengers. As such, ammonium oxalate (AO), benzoquinone (BQ), and isopropanol (IPA) were utilised to trap h^+, $O_2^{\bullet-}$, and $^{\bullet}OH$ radicals, respectively. It is worth mentioning that the radical scavengers were added to the trapping experiments before the addition of H_2O_2 and starting the UV irradiation. Hence, the relevant reactive species can be determined relying on the photocatalytic activity of the catalyst [61]. The photocatalytic activity of $CoAl_2O_4$/C catalyst under different conditions; in the presence and absence of radical scavengers, is displayed in Figure 10. The results revealed that, in the absence of radical scavengers, the removal percentage of MB dye was about 98.5% in 90 min. However, the addition of benzoquinone did not have a significant effect on the photocatalytic degradation of MB dye, and the dye removal percentage was ca. 97%. This indicates that $O_2^{\bullet-}$ radical did not have a significant role in the photocatalytic degradation of MB dye. While, ammonium oxalate and isopropanol, separately, inhibited the reaction remarkably and the degradation reaction was decreased to ca. 69% and 50%, respectively. Therefore, based on the gained results, h^+ and $^{\bullet}OH$ radicals played the main role in the photocatalytic degradation of MB dye.

To further understand the photodegradation mechanism of MB dye in the presence of $CoAl_2O_4$/C catalyst + UV + H_2O_2, we determined the valence band (VB) and conduction band (CB) potentials of the components of the as-prepared nanocomposite. This is also required to illustrate the photogenerated electron-hole pair separation over the as-prepared nanocomposite. Employing the following empirical relationships [62,63], these energy levels were determined, and the results are depicted in Figure 11.

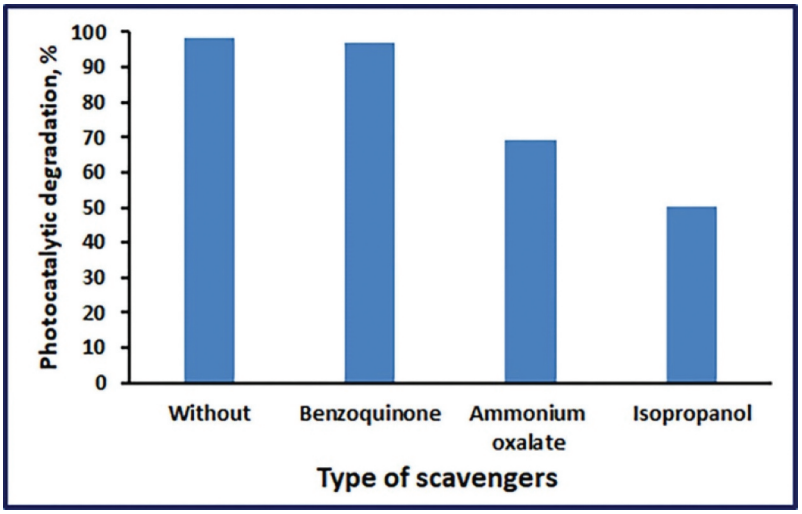

Figure 10. The photocatalytic degradation percentage of MB dye using $CoAl_2O_4/C + H_2O_2 + UV$, in the presence of different scavengers.

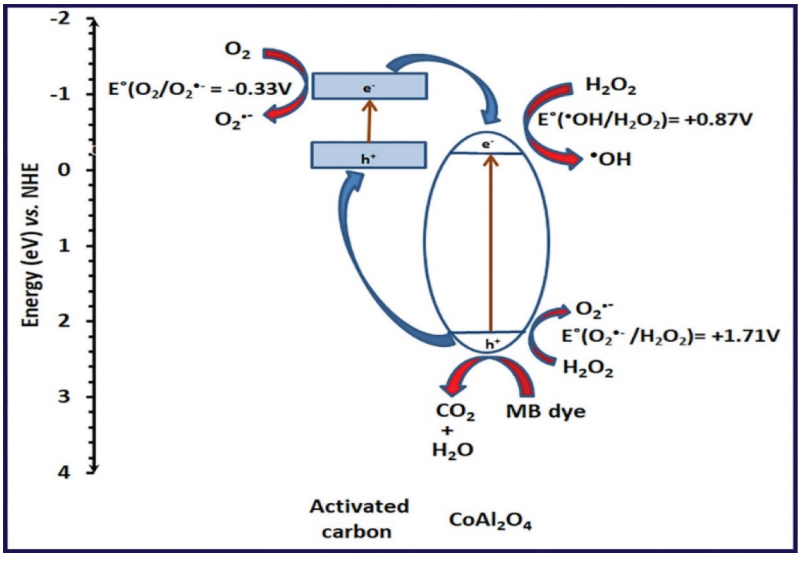

Figure 11. Proposed schematic diagram and photocatalytic degradation of MB dye using $CoAl_2O_4/C + H_2O_2 + UV$.

$$E_{CB} = \chi - E^e - 0.5E_g$$
$$E_{VB} = E_{CB} + E_g$$

where E^e, χ, and E_g are the energy of free electrons on the hydrogen scale (4.5 eV), the absolute electronegativity, and the band gap energy of the nanocomposite. The estimated E_g value for $CoAl_2O_4$ was found to be about 2.2 eV. The calculated VB and

CB energies for $CoAl_2O_4$ were estimated to be 2.062 and −0.138 eV, respectively. In addition, Lim et al reported the energy positions of VB and CB for the carbon thin layer [50].

According to the determined values of VB and CB (Figure 11) for $CoAl_2O_4$ and carbon thin layer, we can propose the photocatalytic degradation of MB dye as following. Under UV irradiation, the electrons in the VBs of $CoAl_2O_4$ and carbon thin layer absorb light and are promoted via excitation to their corresponding CBs. These electrons leave holes (h^+) in the VBs of the $CoAl_2O_4$ and carbon thin layer. In addition, the photogenerated electrons on the carbon thin layer CB flow to $CoAl_2O_4$ CB because the CB energy of the carbon thin layer is more negative than that of the $CoAl_2O_4$ component. Once these charges are formed and separated, they may react with H_2O_2, MB, and/or adsorbed O_2. Some of the photogenerated electrons (e_{CB}^-) in the CB of the carbon thin layer can react with the adsorbed oxygen forming $O_2^{\bullet-}$ reactive species since CB of the carbon thin layer is more negative than the potential of O_2/ $O_2^{\bullet-}$ ($E°(O_2/O_2^{\bullet-})$ = −0.33 V/NHE). This result is consistent with the reported data [64]. Cobalt(II) ions of the spinel oxide may act as a trapping centre for the photogenerated electrons, forming Co(I) ions. These cobalt(I) ions may transport the photogenerated electrons to react with the dissolved oxygen, generating superoxide radical anion. The $O_2^{\bullet-}$ reactive species can be converted into $^{\bullet}OH$ radicals, which enhance the photocatalytic degradation of MB dye (Scheme 2). Similar behaviours were reported by Sumathi et al. for cerium doped zinc aluminate spinel oxide [56]. On the other hand, H_2O_2 is reduced by the photogenerated electrons (e_{CB}^-) of the CB of $CoAl_2O_4$, generating $^{\bullet}OH$ reactive species, which in turn can degrade the MB dye. This is because the CB of $CoAl_2O_4$ is more negative than the potential of $^{\bullet}OH/H_2O_2$ (+0.87 V vs. NHE) [65,66]. In addition, some holes in the VB of $CoAl_2O_4$ may react with H_2O_2 to generate $O_2^{\bullet-}$ radical because this VB is more positive than the potential of $O_2^{\bullet-}/H_2O_2$ (+1.71 V vs. NHE) [65,67]. Some of these holes may also decompose MB molecules through oxidation of the dye into degradation products via aromatic ring-opening mechanism since the UV-Vis spectra of the degradation products did not reveal new bands during the photocatalytic degradation process intermediates [68,69]. Moreover, the reaction of MB dye molecules with the photogenerated $^{\bullet}OH$ and holes bring about dye photodegradation into small molecules such as H_2O and CO_2 [70]. The proposed mechanism is also outlined in Scheme 2.

The degradation of MB dye molecules employing $CoAl_2O_4$/composite+H_2O_2+ UV irradiation can be presented in Scheme 2. In addition, as mentioned previously and displayed in Figure 8(e), the results revealed that performing degradation of MB with $CoAl_2O_4$/C composite + H_2O_2 in the dark resulted in degradation of about 27% after 90 min, and this might be due to heterogeneous Fenton-like reaction. In this light, as shown in Scheme 2, degradation of MB molecules, in this case, can be attributed to the highly reactive free $^{\bullet}OH$ radicals produced through the catalytic decomposition of H_2O_2 by Co^{2+} ions of $CoAl_2O_4$ component. Thereby, the Co^{2+} and H_2O_2 mixture can be regarded as Fenton-like reagent, as reported elsewhere, in which the oxidation-reduction reaction between Co^{2+} and H_2O_2 took place producing $^{\bullet}OH$ radical and Co^{3+} [71]. Thereafter, MB molecules were probably degraded by oxidation by the generated $^{\bullet}OH$ radical and Co^{3+} through this Fenton-like reaction, as outlined in Scheme 2. Similar MB and other dyes catalytic degradation reactions based on the Fenton-like reagents have been reported [72].

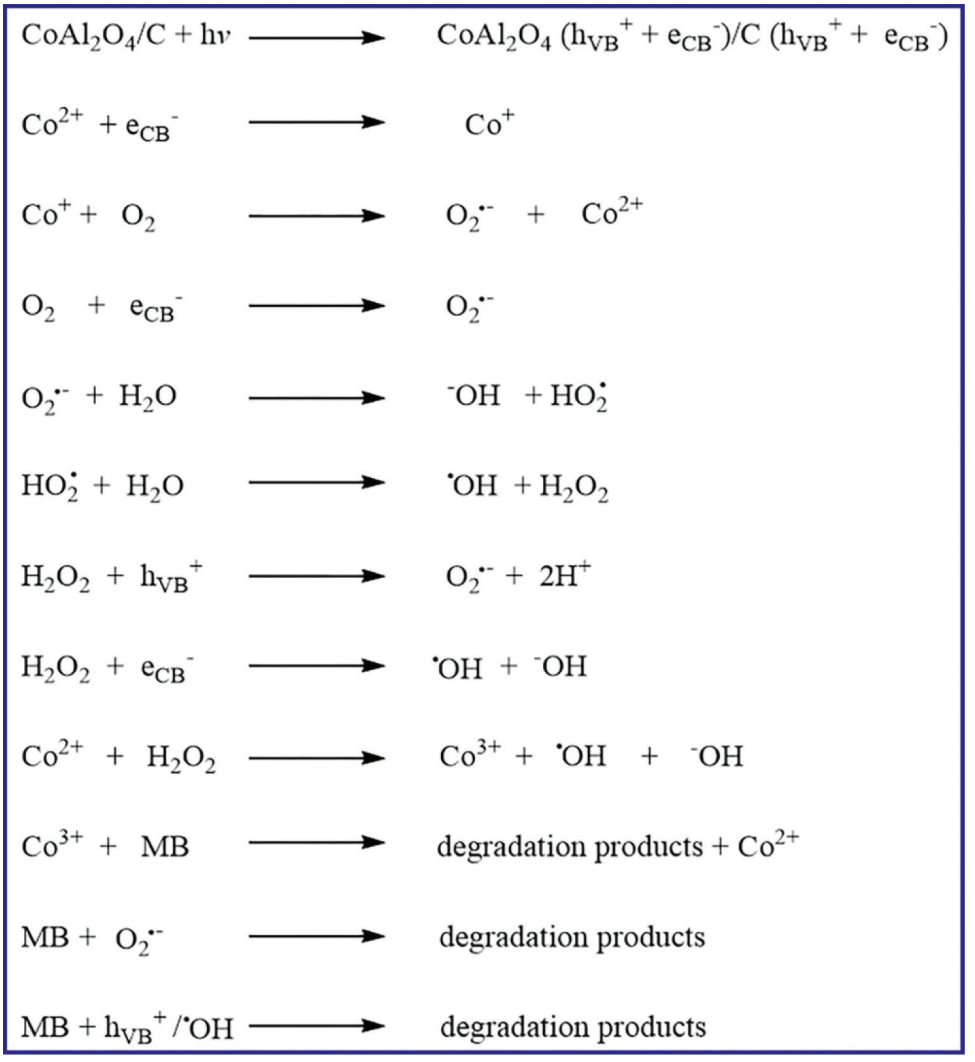

Scheme 2. Proposed photocatalytic degradation of MB dye using $CoAl_2O_4/C$ catalyst + H_2O_2 + UV irradiation.

The efficiency of the as-fabricated $CoAl_2O_4/C$ photocatalyst was examined by investigating its regeneration and reusability for MB dye photodegradation with the help of H_2O_2 under UV irradiation. This investigation was carried out because of its importance from an economic point of view. Therefore, some re-cycling experiments were performed. In this vein, after each cycle, the used photocatalyst was separated, washed with ethanol, and dried at 65°C for 5 h. The results displayed in Figure 12 exhibited that the photocatalytic activity of the as-prepared $CoAl_2O_4/C$ photocatalyst did not show a significant decrease after four cycles, indicating its stability, and it could be reused with reasonable activity as a photocatalyst for at least four times.

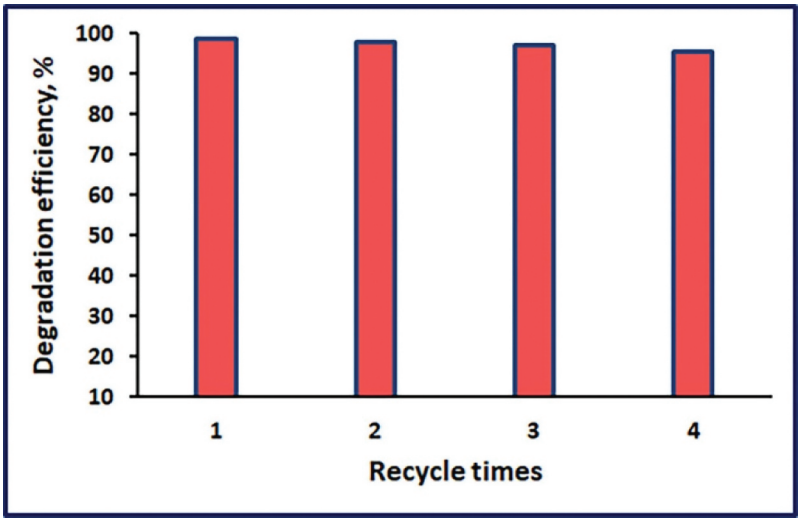

Figure 12. Reusability of the $CoAl_2O_4$/C nanocomposite after four successive runs.

Table 1. Photocatalytic degradation of MB dye using various photocatalysts.

Sample	Irradiation time (min)	MB degradation (%)	Rate constant k (min^{-1})	Reference
Cobalt aluminate	80	37	-	[73]
Graphdiyne-ZnO nanohybrids	120	68	0.00426	[74]
Graphene-ZnO nanofiber mats	240	80	0.006	[75]
Y-doped ZnO	100	90	0.0444	[76]
ZnO@N-C hybrid composite	60	95	0.0456	[77]
Cobalt aluminate/C nanocomposite + 0.4 mL H_2O_2 (30%)	90	98.5	0.046	This study
Nitrogen-doped carbon dot decorated zinc oxide nanoparticles	60	99	0.0557	[78]
ZnO-C nanocomposite	25	99.7	0.1432	[79]

3.4. Comparison with different photocatalysts

Table 1 presents the comparison of the photocatalytic activities of numerous photocatalysts for the catalytic degradation of MB dye. The results exhibited that cobalt aluminate/carbon nanocomposite is superior to several other photocatalysts for the degradation of MB dye. The superiority of the present catalyst is due to the probable low recombination rate of the hole-electron pairs and the high dispersibility of the product. The obtained results also exhibited that the prepared cobalt aluminate/carbon nanocomposite is a promising candidate for the photocatalytic degradation of MB dye under UV light illumination in neutral aqueous solutions.

4. Conclusions

In summary, cobalt aluminate/carbon nanocomposite was successfully synthesised through an auto-combustion procedure utilising a glycine fuel. The product was characterised using different techniques such as X-ray diffraction (XRD), Fourier transform infrared (FT-IR),

thermal analysis (TG), field emission scanning electron microscopy (FE-SEM), transmission electron microscopy (TEM), and X-ray photoelectron spectroscopy (XPS), UV-Vis diffuse reflectance spectrum (DRS), energy-dispersive X-ray spectroscopy (EDS). The methylene blue (MB) dye degradation was investigated under different conditions: (catalyst + dark); (catalyst + UV), (UV only), (H_2O_2 + dark), (H_2O_2 + UV), (catalyst + H_2O_2 + dark), and (catalyst + H_2O_2 + UV) to explore the roles of UV, H_2O_2 and the catalyst in the degradation process. The results exhibited that $CoAl_2O_4$/C photocatalyst in the presence of H_2O_2 under UV irradiation was the most effective in photodecomposition of MB dye which reached about 98.5% in only 90 min of UV irradiation with a degradation rate constant of 0.046 min^{-1}. The holes and $^{\bullet}OH$ radicals are the main reactive species responsible for the degradation process. The photocatalyst showed a good reusability and stability under working conditions.

Acknowledgments

M.M. Aljohani and M.Y. Nassar are thankful to the Deanship of Scientific Research at the University of Tabuk, Saudi Arabia, for the financial support; grant No. S-1441-0029. The last three authors are also thankful to Benha University (http://www.bu.edu.eg/en/), Egypt, for support.

Disclosure statement

No potential conflict of interest was reported by the author(s).

Funding

This work was supported by the Deanship of Scientific Research at University of Tabuk, Saudi Arabia [grant No. S-1441-0029].

ORCID

Mostafa Y. Nassar http://orcid.org/0000-0002-5177-9777

References

[1] M.Y. Nassar, E.I. Ali and E.S. Zakaria, RSC Adv. **7**, 8034 (2017). doi:10.1039/C6RA27924D.
[2] R. Guo, T. Jiao, R. Li, Y. Chen, W. Guo, L. Zhang, J. Zhou, Q. Zhang and Q. Peng, ACS Sustain. Chem. Eng. **6**, 1279 (2018). doi:10.1021/acssuschemeng.7b03635.
[3] M.Y. Nassar, M.M. Moustafa and M.M. Taha, RSC Adv. **6**, 42180 (2016). doi:10.1039/C6RA04855B.
[4] W.-H. Kuan and Y.-C. Chan, J. Hazard. Mater. **239-240**, 152 (2012). doi:10.1016/j.jhazmat.2012.08.051.
[5] J. Fu, Z. Chen, M. Wang, S. Liu, J. Zhang, J. Zhang, R. Han and Q. Xu, Chem Eng Technol **259**, 53 (2015). doi:10.1016/j.cej.2014.07.101.
[6] R. Atchudan, T.N.J.I. Edison, S. Perumal, M. Shanmugam and Y.R. Lee, J. Photochem. Photobiol. A Chem. **337**, 100 (2017). doi:10.1016/j.jphotochem.2017.01.021.
[7] K. Atrak, A. Ramazani and S. Taghavi Fardood, Environ. Technol. **41**, 2760 (2020). doi:10.1080/09593330.2019.1581841.
[8] S. Taghavi Fardood, F. Moradnia, S. Moradi, R. Forootan, F. Yekke Zare and M. Heidari, Nanochem Res **4**, 140 (2019).

[9] N. Arsalani, Y. Panahian and R. Nasiri, Mater Sci Eng B **251**, 114448 (2019). doi:10.1016/j.mseb.2019.114448.
[10] Y. Panahian, N. Arsalani and R. Nasiri, J. Photochem. Photobiol. A Chem. **365**, 45 (2018). doi:10.1016/j.jphotochem.2018.07.035.
[11] R.G. Saratale, G.D. Saratale, J.S. Chang and S.P. Govindwar, J. Taiwan Inst. Chem. Eng. **42**, 138 (2011). doi:10.1016/j.jtice.2010.06.006.
[12] M.Y. Nassar and M. Khatab, RSC Adv. **6**, 79688 (2016). doi:10.1039/C6RA12852A.
[13] M.Y. Nassar and S. Abdallah, RSC Adv. **6**, 84050 (2016). doi:10.1039/C6RA12424K.
[14] J. Niu, A. Wu, D. Wang, L. Zhou, S. Zhang, Z. Liu, P. Feng, X. Ou and Y. Qiang, Mater. Lett. **230**, 32 (2018). doi:10.1016/j.matlet.2018.07.073.
[15] M.F. El-Berry, S.A. Sadeek, A.M. Abdalla and M.Y. Nassar, Mater. Res. Bull. **133**, 111048 (2021). doi:10.1016/j.materresbull.2020.111048.
[16] M.Y. Nassar, A.A. Ali and A.S. Amin, RSC Adv. **7**, 30411 (2017). doi:10.1039/C7RA04899H.
[17] R. Atchudan, T.N.J.I. Edison, S. Perumal, D. Karthikeyan and Y.R. Lee, J. Photochem. Photobiol. B, Biol. **162**, 500 (2016). doi:10.1016/j.jphotobiol.2016.07.019.
[18] K. Atrak, A. Ramazani and S. Taghavi Fardood, J Mater Sci: Mater Electron **29**, 8347 (2018).
[19] Y. Xia, Z. He, J. Su and K. Hu, J Mater Sci: Mater Electron **30**, 9843 (2019).
[20] M.Y. Nassar, I.S. Ahmed and I. Samir, Spectrochim. Acta A Mol. Biomol. Spectrosc. **131**, 329 (2014). doi:10.1016/j.saa.2014.04.040.
[21] H. Tong, S. Ouyang, Y. Bi, N. Umezawa, M. Oshikiri and J. Ye, Adv. Mater. **24**, 229 (2012). doi:10.1002/adma.201102752.
[22] F. Moradnia, S. Taghavi Fardood, A. Ramazani, S. Osali and I. Abdolmaleki, Micro Nano Lett. **15**, 674 (2020). doi:10.1049/mnl.2020.0189.
[23] F. Moradnia, S. Taghavi Fardood, A. Ramazani, B.-K. Min, S.W. Joo and R.S. Varma, J. Clean. Prod. **288**, 125632 (2021). doi:10.1016/j.jclepro.2020.125632.
[24] Z. He, H. Yang, J. Su, Y. Xia, X. Fu, L. Kang, L. Wang and M. Wu, Mater. Lett. **288**, 129375 (2021). doi:10.1016/j.matlet.2021.129375.
[25] M. Pera-Titus, V. García-Molina, M.A. Baños, J. Giménez and S. Esplugas, Appl. Catal. B **47**, 219 (2004). doi:10.1016/j.apcatb.2003.09.010.
[26] Z. He, H. Yang, J. Su, Y. Xia, X. Fu, L. Wang and L. Kang, Fuel **294**, 120399 (2021). doi:10.1016/j.fuel.2021.120399.
[27] M. Yang and J. He, J. Colloid Interface Sci. **355**, 15 (2011). doi:10.1016/j.jcis.2010.11.022.
[28] G. Zhang, S. Wang, S. Zhao, L. Fu, G. Chen and F. Yang, Appl. Catal. B **106**, 370 (2011). doi:10.1016/j.apcatb.2011.05.042.
[29] C.S. Zalazar, M.L. Satuf, O.M. Alfano and A.E. Cassano, Environ. Sci. Technol. **42**, 6198 (2008). doi:10.1021/es800028h.
[30] C. Li, J. Ma, J. Shen and P. Wang, J. Hazard. Mater. **166**, 891 (2009). doi:10.1016/j.jhazmat.2008.11.111.
[31] M.O. Uslu, M.F. Rahman, S.Y. Jasim, E.K. Yanful and N. Biswas, Water Air Soil Pollut. **223**, 3173 (2012). doi:10.1007/s11270-012-1099-3.
[32] H. Niu, D. Zhang, S. Zhang, X. Zhang, Z. Meng and Y. Cai, J. Hazard. Mater. **190**, 559 (2011). doi:10.1016/j.jhazmat.2011.03.086.
[33] L. Hou, Q. Zhang, F. Jérôme, D. Duprez, H. Zhang and S. Royer, Appl. Catal. B **144**, 739 (2014). doi:10.1016/j.apcatb.2013.07.072.
[34] A.R. Yeddou, S. Chergui, A. Chergui, F. Halet, A. Hamza, B. Nadjemi, A. Ould-Dris and J. Belkouch, Miner Eng **24**, 788 (2011). doi:10.1016/j.mineng.2011.02.012.
[35] Y. Xu, Z. Lin, Y. Zheng, J.-P. Dacquin, S. Royer and H. Zhang, Sci. Total Environ. **651**, 2585 (2019). doi:10.1016/j.scitotenv.2018.10.005.
[36] A. Movasati, S.M. Alavi and G. Mazloom, Fuel **236**, 1254 (2019). doi:10.1016/j.fuel.2018.09.069.
[37] V.S. Kirankumar and S. Sumathi, Mater Today Chem **18**, 100355 (2020). doi:10.1016/j.mtchem.2020.100355.
[38] M. Karmaoui, N.J.O. Silva, V.S. Amaral, A. Ibarra, Á. Millán and F. Palacio, Nanoscale **5**, 4277 (2013). doi:10.1039/c3nr34229h.

[39] V.S. Kirankumar and S. Sumathi, Mater. Chem. Phys. **197**, 17 (2017). doi:10.1016/j.matchemphys.2017.05.021.
[40] C. Ragupathi, J. Judith Vijaya, S. Narayanan, S.K. Jesudoss and L. John Kennedy, Ceram Int **41**, 2069 (2015). doi:10.1016/j.ceramint.2014.10.002.
[41] I. Mindru, G. Marinescu, D. Gingasu, L. Patron, C. Ghica and M. Giurginca, Mater. Chem. Phys. **122**, 491 (2010). doi:10.1016/j.matchemphys.2010.03.032.
[42] R. Chellammal Gayathri, V. Elakkiya and S. Sumathi, Inorg. Chem. Commun. **129**, 108634 (2021). doi:10.1016/j.inoche.2021.108634.
[43] M. Dhinagaran, V. Elakkiya and S. Sumathi, Opt Mater (Amst) **111**, 110546 (2021). doi:10.1016/j.optmat.2020.110546.
[44] J. Lu, K. Minami, S. Takami and T. Adschiri, Chem. Eng. Sci. **85**, 50 (2013). doi:10.1016/j.ces.2012.01.061.
[45] S. Kurajica, J. Popović, E. Tkalčec, B. Gržeta and V. Mandić, Mater. Chem. Phys. **135**, 587 (2012). doi:10.1016/j.matchemphys.2012.05.030.
[46] V. Elakkiya, Y. Agarwal and S. Sumathi, Solid State Sci **82**, 92 (2018). doi:10.1016/j.solidstatesciences.2018.06.008.
[47] S. Salem, J Indus Eng Chem **20**, 818 (2014). doi:10.1016/j.jiec.2013.06.011.
[48] V.S. Kirankumar, N. Mayank and S. Sumathi, J. Taiwan Inst. Chem. Eng. **95**, 602 (2019). doi:10.1016/j.jtice.2018.09.020.
[49] Y. He, Y. Cao, H. Liao and J.-A. Wang, Powder Technol **324**, 95 (2018). doi:10.1016/j.powtec.2017.08.056.
[50] H.-S. Lim, J. Lee, S. Lee, Y.S. Kang, Y.-K. Sun and K.-D. Suh, Acta Mater **122**, 287 (2017). doi:10.1016/j.actamat.2016.09.031.
[51] S.R. Jain, K.C. Adiga and V.R. Pai Verneker, Combust Flame **40**, 71 (1981). doi:10.1016/0010-2180(81)90111-5.
[52] R. Jenkins and R.L. Snyder, *Introduction to X-ray Powder Diffractometry* (John Wiley & Sons, Inc., New York, 1996).
[53] M.M. Sobeih, M.F. El-Shahat, A. Osman, M.A. Zaid and M.Y. Nassar, RSC Adv. **10**, 25567 (2020). doi:10.1039/D0RA02340J.
[54] K. Nakamoto, *Infrared and Raman Spectra of Inorganic and Coordination Compounds, Part B: Applications in Coordination, Organometallic, and Bioinorganic Chemistry, 6th* Ed (Wiley-Interscience, New Jersey, 2009).
[55] I. Mindru, D. Gingasu, L. Patron, A. Ianculescu, V.-A. Surdu, D.C. Culita, S. Preda, C.-D. Negut and O. Oprea, Mater Sci Eng B **246**, 42 (2019). doi:10.1016/j.mseb.2019.05.031.
[56] S. Sumathi and A. Kavipriya, Solid State Sci **65**, 52 (2017). doi:10.1016/j.solidstatesciences.2017.01.003.
[57] X. Peng, J. Cheng, J. Yuan, N. Jin, J. Kang, Y. Hou and Q. Zhang, Adv Appl Ceram **117**, 303 (2018). doi:10.1080/17436753.2017.1410941.
[58] A. Roniboss, A. Subramani, R. Ramamoorthy, S. Yuvaraj, M. Sundararajan and C.S. Dash, Mater Sci Semicond Process **123**, 105507 (2021). doi:10.1016/j.mssp.2020.105507.
[59] S. Taghavi Fardood, R. Forootan, F. Moradnia, Z. Afshari and A. Ramazani, Mater. Res. Express **7**, 015086 (2020). doi:10.1088/2053-1591/ab6c8d.
[60] Y. El Jabbar, M. ElHafdi, M. Benchikhi, R. El Ouatib, L. Er-Rakho and A. Essadki, Environ Nanotechnol Monit Manag **12**, 100259 (2019). doi:10.1016/j.enmm.2019.100259.
[61] Z. He, J. Su, Y. Xia and B. Tang, Micro Nano Lett. **15**, 499 (2020). doi:10.1049/mnl.2020.0016.
[62] M.A. Butler and D.S. Ginley, J. Electrochem. Soc. **125**, 228 (1978). doi:10.1149/1.2131419.
[63] Y. Xu and M.A.A. Schoonen, Am. Mineral. **85**, 543 (2000). doi:10.2138/am-2000-0416.
[64] I. Velo-Gala, J.J. López-Peñalver, M. Sánchez-Polo and J. Rivera-Utrilla, Appl. Catal. B **142-143**, 694 (2013). doi:10.1016/j.apcatb.2013.06.003.
[65] B.H.J. Bielski, D.E. Cabelli, R.L. Arudi and A.B. Ross, J Phys Chem Ref Data **14**, 1041 (1985). doi:10.1063/1.555739.
[66] A.C. Da Silva, M.R. Almeida, M. Rodriguez, A.R.T. Machado, L.C.A. de Oliveira and M.C. Pereira, J. Photochem. Photobiol. A Chem. **332**, 54 (2017). doi:10.1016/j.jphotochem.2016.08.013.

[67] T. Hirakawa, K. Yawata and Y. Nosaka, Appl. Catal. A Gen. **325**, 105 (2007). doi:10.1016/j.apcata.2007.03.015.
[68] B. Golzad-Nonakaran and A. Habibi-Yangjeh, Adv Powder Technol **27**, 1427 (2016). doi:10.1016/j.apt.2016.05.001.
[69] A. Akhundi and A. Habibi-Yangjeh, Ceram Int **41**, 5634 (2015). doi:10.1016/j.ceramint.2014.12.145.
[70] J. Zhang and Z. Ma, RSC Adv. **7**, 2163 (2017). doi:10.1039/C6RA26352F.
[71] S. Goldstein, D. Meyerstein and G. Czapski, Free Radic. Biol. Med. **15**, 435 (1993). doi:10.1016/0891-5849(93)90043-T.
[72] J. Liao, H. Li, X. Zhang, D. Xiao and N. Qiang, Appl. Catal. A Gen. **491**, 94 (2015). doi:10.1016/j.apcata.2014.11.042.
[73] T. Gholami, M. Salavati-Niasari and S. Varshoy, Int. J. Hydrogen Energy **41**, 9418 (2016). doi:10.1016/j.ijhydene.2016.03.144.
[74] S. Thangavel, K. Krishnamoorthy, V. Krishnaswamy, N. Raju, S.J. Kim and G. Venugopal, J. Phys. Chem. C **119**, 22057 (2015). doi:10.1021/acs.jpcc.5b06138.
[75] S. An, B.N. Joshi, M.W. Lee, N.Y. Kim and S.S. Yoon, Appl. Surf. Sci. **294**, 24 (2014). doi:10.1016/j.apsusc.2013.12.159.
[76] P.K. Sanoop, S. Anas, S. Ananthakumar, V. Gunasekar, R. Saravanan and V. Ponnusami, Arab J Chem **9**, S1618–S1626 (2016). doi:10.1016/j.arabjc.2012.04.023.
[77] R. Atchudan, T.N.J.I. Edison, S. Perumal, N. Karthik, D. Karthikeyan, M. Shanmugam and Y.R. Lee, J. Photochem. Photobiol. A Chem. **350**, 75 (2018). doi:10.1016/j.jphotochem.2017.09.038.
[78] R. Atchudan, T.N.J.I. Edison, S. Mani, S. Perumal, R. Vinodh, S. Thirunavukkarasu and Y.R. Lee, Dalton Trans **49**, 17725 (2020). doi:10.1039/D0DT02756A.
[79] J. Xue, S. Ma, Y. Zhou and Z. Zhang, New J Chem **39,** 1852 (2015). doi:10.1039/C4NJ02004A.